Clim Dyn
DOI 10.1007/s00382-011-1281-0

Impacts of upscale heat and momentum transfer by moist Kelvin waves on the Madden–Julian oscillation: a theoretical model study

Fei Liu · Bin Wang

Received: 11 October 2011 / Accepted: 23 December 2011

Abstract The Madden–Julian oscillation (MJO) is observed to interact with moist Kelvin waves. To understand the role of this interaction, a simple scale-interaction model is built, which describes the MJO modulation of moist Kelvin waves and the feedback from moist Kelvin waves through upscale eddy heat and momentum transfer. The backward-tilted moist Kelvin waves produce eddy momentum transfer (EMT) characterized by the lower-tropospheric westerly winds and eddy heat transfer (EHT) that warms the mid-troposphere. The EHT tends to induce the lower-tropospheric easterly winds and low pressure, which is located in front of the "westerly wind burst" induced by the EMT. Adding the eddy forcing to a neutral MJO skeleton model, we show that the EHT provides an instability source for the MJO by warming up the mid-troposphere, and the EMT offers an additional instability source by enhancing the lower-tropospheric westerly winds. The eddy forcing selects eastward propagation for the unstable mode, because it generates positive/negative eddy available potential energy for the eastward/westward modes by changing their thermal and dynamical structures. The present results show that moist Kelvin waves can provide a positive feedback to the MJO only when they are located within (or near) the convective complex (center) of the MJO. The EHT and EMT feedback works positively in the front and rear part of the MJO, respectively. These theoretical results suggest the potential importance of moist Kelvin waves in sustaining the MJO and encourage further observations to document the relationship between moist Kelvin waves and the MJO.

Keywords Madden–Julian oscillation · Moist Kelvin waves · Scale interaction · Eddy heat transfer · Eddy momentum transfer

1 Introduction

The dominant mode of the tropical intraseasonal oscillation, the Madden–Julian oscillation (MJO) (Madden and Julian 1971, 1972, 1994), is a slowly eastward propagating, planetary-scale envelope of convectively coupled equatorial waves (Nakazawa 1988; Straub and Kiladis 2003; Haertel and Kiladis 2004; Moncrieff 2004; Kikuchi and Wang 2010). For example, the quasi 2-day waves are usually observed to be enhanced in the front part of the MJO (Kikuchi and Wang 2010), while moist Kelvin waves can travel through the MJO envelope: They can occur in the rear part, the Rossby wave-gyre region of the MJO (Lin and Johnson 1996; Moncrieff and Klinker 1997; Houze et al. 2000), or in the front part of the MJO (Roundy 2008; Kikuchi and Wang 2010).

A series of recent works have been carried out to understand the scale interaction between the MJO and convectively coupled equatorial waves. For the westward propagating, convectively coupled equatorial waves, especially the 2-day waves, it is now clear that their eddy momentum transfer (EMT) can help to generate the anti-cyclonic pair of the quadrupole vortex in the front part of the MJO (Biello and Majda 2005; Wang and Liu 2011) and provides an instability source for the MJO (Wang and Liu

F. Liu · B. Wang
International Pacific Research Center, University of Hawaii at Manoa, Honolulu, HI, USA

B. Wang (✉)
Department of Meteorology, University of Hawaii at Manoa, 401 POST Bldg, 1680 East–West Road, Honolulu, HI 96822, USA
e-mail: wangbin@hawaii.edu

Published online: 15 February 2012

2011; Liu and Wang 2011; Liu et al. 2011); on the other hand, the eddy heat transfer (EHT) of 2-day waves provides a negative feedback to the MJO (Liu and Wang 2011). For the eastward propagating convectively coupled waves such as moist Kelvin waves, the EMT of synoptic-scale motions can maintain the horizontal quadrupole-vortex structure and vertical westerly-wind-burst structure of the MJO (Majda and Biello 2004; Biello and Majda 2005; Wang and Liu 2011). Moreover, it produces an intraseasonal variability of planetary-scale winds (Majda and Stechmann 2009a) and provides an instability source for sustaining the MJO (Wang and Liu 2011). Although these works demonstrated the role of the EMT, they were done by using models that did not fully cope with the observational records in various crucial ways.

Furthermore, the role of the EHT associated with moist Kelvin waves has not been addressed in MJO dynamics. To understand the interaction between moist Kelvin waves and the MJO, it is necessary to find out how moist Kelvin waves affect the MJO through their EHT, especially when the EHT couples with the EMT. Further, since moist Kelvin waves usually travel through the MJO envelope, will moist Kelvin waves affect the MJO differently when they are located in different parts of the MJO?

In order to study the interaction between moist Kelvin waves and the MJO, we try to build a scale-interaction dynamical model, which includes two essential physical processes: (a) the convective complex of the MJO modulates the strength and location of moist Kelvin waves, and (b) moist Kelvin waves feed back to the MJO through the upscale EMT and EHT. Such a dynamical framework is presented in Sect. 2. In Sect. 3 we derive the EMT and EHT based on dynamical and thermal structures of moist Kelvin waves under specified heat forcing. The planetary-scale responses to the forcing of moist Kelvin waves are calculated with a specified envelope of moist Kelvin waves (Sect. 4). Based on the results in Sects. 3 and 4, we further parameterize the eddy flux envelope of moist Kelvin waves and obtain a scale-interaction model (Sect. 5). The results derived from this scale-interaction model are discussed in Sect. 6. This paper ends up with a discussion in the last section.

2 The dynamical model

The dynamical model used in this work is mainly based on the intraseasonal planetary equatorial synoptic dynamics (IPESD) model that was derived by Majda and Klein (2003), in which the dynamics of planetary-scale and synoptic-scale motions are separated. The IPESD takes Boussinesq equations with a standard tropospheric value for the buoyancy frequency, $N = 10^{-2}$ s^{-1}. When the role of the boundary layer and stratosphere is ignored, the rigid lid boundary conditions were used with no vertical flows at the bottom (at 0.5 km) and top (at 16.5 km) of the free troposphere. The natural reference speed, c_{ref}, is selected as the gravity wave speed of the first baroclinic mode, $c = 50$ m s^{-1}. Then the standard equatorial synoptic length and time scales, l_s, T_s, are defined by $l_s = (c/\beta)^{1/2} = 1{,}500$km and $T_s = (c\beta)^{-1/2} = 8.5$h, respectively, where β represents the leading order curvature effect of the Earth at the equator. Since the reference speed, $c = 50$ m s^{-1}, is large for the wind speed, it is suitable to introduce the Froude number, defined by the ratio of the typical horizontal wind magnitude and the reference speed, $F_r = v_{\text{ref}}/c = \varepsilon$. The small Froude number, $0.1 \leq \varepsilon \leq 0.4$, gives reasonable flow velocities for the tropical tropospheric motion.

Assume that the synoptic motion occurs with characteristic scales of length, l_s, and time, T_s, and the planetary-scale motion has a length scale, l_s/ε, and a time scale, $T_I = l_s/v_{\text{ref}} \approx 3$ days, respectively, Majda and Klein (2003) obtained the simplified multi-scale equations, i.e., the IPESD equations. The IPESD model has a reasonable scale for equatorial synoptic-scale dynamics with zonal-wind velocities of order 10 m s^{-1} and associated convective heating with a magnitude of 10 K day^{-1}. The scale parameters are listed in Table 1, which are same as those used by Biello and Majda (2005).

In observations (Wheeler and Kiladis 1999), the MJO usually spans wavenumber 1 and 2 with a period of 30–60 days, while moist Kelvin waves span wavenumber 4 through 8 with a period under 10 days. So it is reasonable to think of an MJO modulation of equatorial Kelvin waves.

Table 1 List of scale parameters in the IPESD model

Physical quantity	Name	Value or unit scale
Equatorial β-parameter	$(\beta = f_y)$	2.3×10^{-11} (m s)$^{-1}$
Froude number	ε	0.125
Reference wave speed	c	50 m s^{-1}
Synoptic time scale	T_s	$(c\beta)^{-1/2} = 8.3$ h
Equatorial deformation radius	l_s	$(c/\beta)^{1/2} = 1{,}500$ km
Troposphere height	H_T	16 km
Synoptic-scale dimensions	$[x, y]$	$l_s = 1{,}500$ km
Vertical dimension	$[z]$	$H = H_T/\pi = 5$ km
Planetary zonal scale	$[X]$	$l_s/\varepsilon = 12{,}000$ km
Planetary advection time	$[t]$	$T_I \equiv T_s/\varepsilon \approx 3$ days
Horizontal velocity scale	$[u', v', \overline{U}]$	$\varepsilon C = 6.25$ ms^{-1}
Vertical velocity scale	$[w']$	$\varepsilon CH/l_s = 2.5$ cms^{-1}
Temperature scale	$[\theta', \overline{\theta}]$	3 K
Pressure scale	$[p', \overline{P}]$	$\varepsilon C^2 = 312$ m^{2}s^{-2}
Synoptic-scale heating rate	$[S^{\theta\prime}]$	10 K day^{-1}
Planetary-scale heating rate	$[S^{\Theta}]$	1.25 K day^{-1}

The planetary scales associated with the MJO are $X = \varepsilon x$, and $t = \varepsilon\tau$, where x and τ are synoptic-scale zonal and temporal disturbances, respectively. Here we select $\varepsilon = 0.125$ (Majda and Biello 2004; Biello and Majda 2005).

In the IPESD model, U, V, W denote the x, y, z (zonal, meridional, and vertical) components of velocities, respectively, and the remaining dynamic variables are the pressure, P, and the potential temperature, θ. The dynamic variables can be separated into the large-scale envelope means associated with the MJO (the bar quantities) and the synoptic-scale fluctuations associated with moist Kelvin waves (the primes). Thus, the temperature, pressure, and velocities are expressed (Biello and Majda 2006)

$$\begin{aligned}
\theta &= \overline{\theta}(\varepsilon x, y, z, \varepsilon\tau) + \theta\prime(\varepsilon x, x, y, z, \varepsilon\tau, \tau) + O(\varepsilon),\\
P &= \overline{P}(\varepsilon x, y, z, \varepsilon\tau) + p\prime(\varepsilon x, x, y, z, \varepsilon\tau, \tau) + O(\varepsilon),\\
U &= \overline{U}(\varepsilon x, y, z, \varepsilon\tau) + u\prime(\varepsilon x, x, y, z, \varepsilon\tau, \tau) + O(\varepsilon),\\
V &= \varepsilon\overline{V}(\varepsilon x, y, z, \varepsilon\tau) + v\prime(\varepsilon x, x, y, z, \varepsilon\tau, \tau) + O(\varepsilon),\\
W &= \varepsilon\overline{W}(\varepsilon x, y, z, \varepsilon\tau) + w\prime(\varepsilon x, x, y, z, \varepsilon\tau, \tau) + O(\varepsilon).
\end{aligned} \tag{1}$$

The expansion in Eq. 1 is nondimensionalized by the synoptic length scale l_s and time scale T_s, and the planetary length scale l_s/ε and time scale T_l. Meanwhile, the troposphere height defines the vertical length scale so that vertical motions are much weaker than horizontal motions. In Eq. 1, the average over the equatorial synoptic scale of a general function $g(\varepsilon x, x, y, z, \varepsilon\tau, \tau)$ is defined by

$$\overline{g}(X, y, z, t) = \lim_{L\to\infty}\lim_{T\to\infty}\frac{1}{4LT}\int_{-T}^{T}\int_{-L}^{L} g(\varepsilon x, x, y, z, \varepsilon\tau, \tau)dxd\tau, \tag{2}$$

where L and T are the zonal and time sales of the large-scale envelope, respectively. The synoptic-scale equations for the moist Kelvin waves ($v' = 0$) satisfy:

$$\begin{aligned}
&u'_\tau + p'_x = 0,\\
&yu' + p'_y = 0,\\
&u'_x + w'_z = 0,\\
&p'_z = \theta',\\
&\theta'_\tau + w' = S^{\theta\prime}, \overline{S^{\theta\prime}} = 0,
\end{aligned} \tag{3}$$

where $S^{\theta\prime}$ is the heating rate of moist Kelvin waves. The large-scale envelope satisfies the quasi-linear, equatorial long-wave approximation and the equations

$$\begin{aligned}
&\overline{U}_t - y\overline{V} + \overline{P}_X = F^U - d\overline{U},\\
&y\overline{U} + \overline{P}_y = 0,\\
&\overline{P}_z = \overline{\theta},\\
&\overline{U}_X + \overline{V}_y + \overline{W}_z = 0,\\
&\overline{\theta}_t + \overline{W} = S^{\Theta} + F^{\theta} - d_\theta\overline{\theta},
\end{aligned} \tag{4}$$

where S^{Θ} is the planetary-scale mean heating rate. d and d_θ are the momentum and thermal damping coefficients, respectively. Here the same damping scale of 15 days (nondimensional $d = d_\theta \approx 0.18$) is used. Two eddy forcing, the EMT, F^U, and EHT, F^θ, are calculated from the turbulent momentum and temperature fluxes,

$$\begin{aligned}
F^U &= -\overline{(u'v')}_y - \overline{(u'w')}_z,\\
F^\theta &= -\overline{(\theta'v')}_y - \overline{(\theta'w')}_z.
\end{aligned} \tag{5}$$

3 Moist Kelvin waves

3.1 The structures of moist Kelvin waves

The observed moist Kelvin waves have zonal wind perturbations in phase with their pressure field (Takayabu and Murakami 1991). They have horizontal convective scale of 1,500–3,000 km, and eastward phase speed of 15–20 m s^{-1} (Nakazawa 1988; Wheeler and Kiladis 1999). Usually, the moist Kelvin waves are strongly coupled with the stratiform clouds and deep convection and exhibit a westward tilt (Kiladis et al. 2009). Here we do not include the congestus clouds of moist Kelvin waves, which do not affect their vertical structure and associated eddy fluxes essentially (Biello and Majda 2005).

Following the idea of Majda and Biello (2004) that the westward tilt comes from the phase lag between the stratiform clouds and deep convection, we specify the cloud structures of moist Kelvin waves such that the stratiform clouds tail (in the direction of eastward propagation) the deep convection by a phase ϕ_0. In the troposphere, the stratiform heating warms up the upper troposphere but cools down the lower troposphere, and the deep convective heating warms up the middle troposphere, so the total cloud heating can be parameterized as sum of the first baroclinic mode ($j = 1$) associated with the deep convection and the second baroclinic mode ($j = 2$) associated with the stratiform clouds (Mapes 2000; Khouider and Majda 2006, 2007; Waite and Khouider 2009). The heating term in Eq. 3 can be represented by

$$S^{\theta\prime} = F(X, t)\sum_{j=1,2} Q_j \cos(kx - kC_r\tau + \phi_j)\sin(jz), \tag{6}$$

where k and C_r are the wavenumber and phase speed of moist Kelvin waves, respectively. We assume that the stratiform and deep convective heating have the same horizontal structure. $k = 3.15$ is selected for a dimensional zonal convective scale of 3,000 km, and $C_r = 0.36$ is selected for a dimensional eastward phase speed of 18 m s^{-1}. $\phi_1 = 0$, and $\phi_2 = \phi_0$, which means that the stratiform heating tails the deep convective heating by a phase of ϕ_0. In this work we use $\phi_0 = \pi/3$. The strength of

stratiform heating is assumed to be two thirds of that of deep convective heating, $Q_2 = -2Q_1/3$. $F(X, t)$ is the envelope of moist Kelvin waves.Forced by this heating rate Eq. 6, the synoptic-scale variables in Eq. 3 can be separated into the first ($j = 1$) and second ($j = 2$) baroclinic modes

$$\begin{aligned}\{u', v', p'\} &= F(X,t)\sum_{j=1,2}\{u'_j, v'_j, p'_j\}\cos(jz),\\ \{\theta', w'\} &= F(X,t)\sum_{j=1,2}\{\theta'_j, w'_j\}\sin(jz).\end{aligned} \tag{7}$$

Substitution of Eq. 7 into Eq. 3 gives the jth mode of moist Kelvin waves

$$\begin{aligned}&u'_{j\tau} + p'_{jx} = 0,\\ &yu'_j + p'_{jy} = 0,\\ &u'_{jx} + jw'_j = 0,\\ &\theta'_j = -jp'_j,\\ &\theta'_{j\tau} + w'_j = S_j^{\theta\prime}.\end{aligned} \tag{8}$$

To solve these moist Kelvin waves under the specified heat forcing Eq. 6, we apply the idea of reduced stability to Eq. 8 and assume that the diabatic heating comes from the moisture convergence

$$S_j^{\theta\prime} = H_j w'_j, \tag{9}$$

where H_j is an arbitrary positive constant. The negative heating is a simplification for dealing with the anomalous heating. Since the stratiform clouds and deep convection of moist Kelvin waves are assumed to have same zonal structure of $\cos(kx - kC_r\tau + \phi_j)$, we introduce this structure into Eqs. 8–9 and obtain a set of standard equations for the Kelvin wave (Matsuno 1966), which has an equivalent depth of 29.5 m. So the solution for the jth mode can be written as

$$\begin{aligned}\{u'_j, w'_j, \theta'_j, p'_j\} &= \frac{Q_j}{H_j}D_0\Big\{-\frac{j}{k}\sin(kx - kC_r\tau + \phi_j),\\ &\cos(kx - kC_r\tau + \phi_j), \frac{j^2C_r}{k}\sin(kx - kC_r\tau + \phi_j),\\ &-\frac{jC_r}{k}\sin(kx - kC_r\tau + \phi_j)\Big\}.\end{aligned} \tag{10}$$

For the specified phase speed C_r, the positive constant H_j is determined as

$$H_j = 1 - j^2C_r^2, \tag{11}$$

where $H_1 = 0.9$ and $H_2 = 0.5$.

The meridional structure of waves is given in terms of parabolic cylinder functions (D), which take the form of

$$D_s = \exp[-(y/2\sqrt{C_r})^2]P_s(y/\sqrt{C_r}), \tag{12}$$

where P_s is a polynomial of order s.

The total solution of moist Kelvin waves is composed of these two vertical modes:

$$\begin{aligned}\begin{Bmatrix}u'\\ p'\end{Bmatrix} &= F(X,t)\sum_{j=1,2}\frac{Q_j}{H_j}\begin{Bmatrix}-\frac{j}{k}\sin(kx - C_r\tau + \phi_j)\\ -\frac{jC_r}{k}\sin(kx - C_r\tau + \phi_j)\end{Bmatrix}\cos(jz)D_0,\\ \begin{Bmatrix}w'\\ \theta'\end{Bmatrix} &= F(X,t)\sum_{j=1,2}\frac{Q_j}{H_j}\begin{Bmatrix}\cos(kx - C_r\tau + \phi_j)\\ \frac{j^2C_r}{k}\sin(kx - C_r\tau + \phi_j)\end{Bmatrix}\sin(jz)D_0.\end{aligned} \tag{13}$$

For example, the envelope of moist Kelvin waves can be defined as

$$\begin{aligned}&F(X,t) = \cos(\pi(X - 180^\circ)/2L_F) \quad \text{when} \quad |X - 180^\circ| \le L_F,\\ &F(X,t) = 0 \quad \text{when} \quad |X - 180^\circ| > L_F.\end{aligned} \tag{14}$$

This envelope spans 90° with center at 180° when $L_F = 45°$. In this work, this envelope does not depend on the time except in the scale-interaction model (Sects. 5 and 6).

Figure 1 exhibits the snapshot of vertical and horizontal structures of moist Kelvin waves at time 0. Above the equator, the moist Kelvin waves appear as a train of synoptic waves with upward vertical and westward tilt (Fig. 1a), a similar structure with that presented by Majda and Biello (2004) for the super cloud clusters in the warm pool. This solution also yields a similar horizontal structure (Fig. 1b) with the observed Kelvin waves (Fig. 7 of Kiladis et al. 2009), in which the positive temperature anomalies lead the wave convergence, and all disturbances are equatorially trapped (Fig. 1b).

3.2 The EMT and EHT

Substitution of Eq. 13 into 5 yields the explicit momentum and thermal forcing, and the EMT and EHT are given by

$$\begin{aligned}F^U &= \kappa F(X,t)^2D_0^2[\cos(z) - \cos(3z)],\\ F^\theta &= \kappa C_r F(X,t)^2D_0^2[\sin(z) - 3\sin(3z)],\end{aligned} \tag{15}$$

where

$$\kappa = -\frac{3}{4}\frac{Q_1Q_2}{kH_1H_2}\sin(\phi_0). \tag{16}$$

In the convective envelope of the MJO, although the fast ($\approx$18 m s^{-1}) moist Kelvin waves travel as a high-frequency wave train (Fig. 1a), which has zero mean of thermal and momentum variables on planetary scales and depends on the time, they do produce upscale eddy flux transfer that only depends on the characteristics of moist Kelvin waves, such as the vertical tilt, ϕ_0, the heating magnitude, Q_j, the zonal scale, k, and the phase speed, C_r. This means that *the eddy flux transfer is only determined by the type rather than the details of moist Kelvin waves*.

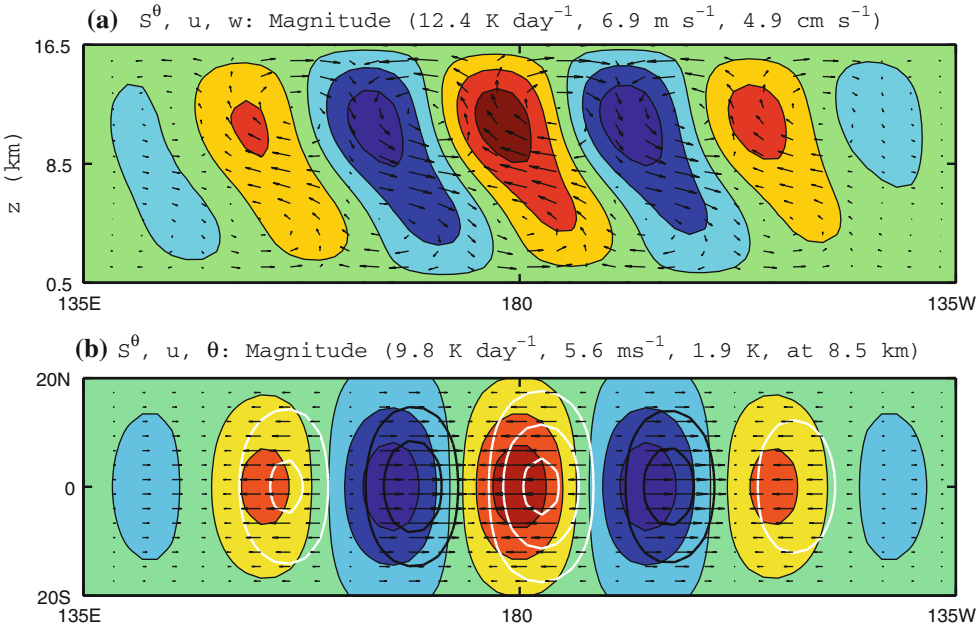

Fig. 1 Vertical (backward-tilted) and horizontal (equatorially trapped) structures of moist Kelvin waves simulated in the model. **a** Vertical distribution of the synoptic-scale heating (*red*)/cooling (*blue*), and velocity (vectors) above the equator as functions of x and z for the westward-tilted (ϕ_0) moist Kelvin waves. **b** Horizontal heating (*red shading*), cooling (*blue shading*), positive temperature (*white contours*), negative temperature (*black contours*), and velocity (vectors) at height 8.5 km. Contour interval is one-third of the magnitude and zero contours are not drawn. The magnitudes for each field are indicated on the *top* of each panel

Because of their pronounced westward tilt, the moist Kelvin waves produce the lower-tropospheric westerly and upper-tropospheric easterly EMT (Fig. 2a), both of which have their maxima trapped at the equator. Figure 2b shows that the moist Kelvin waves also present strong EHT, which tends to warm up the middle troposphere, while cools down the upper and lower troposphere. From Eq. 15, the EHT has the same meridional structure as the EMT, and is equatorially trapped.

For a standard moist Kelvin wave train that has a first baroclinic heating rate of 10 K day^{-1} at its maximum, a second baroclinic heating rate of 6.7 K day^{-1} at its maximum, a zonal convective scale of 3,000 km, and a phase lag of 500 km between the stratiform clouds and deep convection, the EMT, F^U, produces a westerly wind acceleration whose maximum is 3.2 m s^{-1} day^{-1} at height 4.5 km above the equator (Fig. 2a). Meanwhile, the EHT, F^θ, produces a heating acceleration whose maximum is 1.4 K day^{-1} at the middle troposphere above the equator (Fig. 2b). It is worth mentioning that the EHT has amplitude that is comparable to the EMT, and their nondimensional amplitude ratio can reach 0.9 under current heat forcing.

In order to study the role of moist Kelvin waves in the MJO, we try to build a simple scale-interaction model that only explains the first baroclinic mode of the MJO, and the EMT and EHT of moist Kelvin waves can be easily parameterized by the first baroclinic features of the MJO, so we truncate the EMT and EHT to the first baroclinic mode and study their characteristics. The eddy fluxes are written easily on the first baroclinic mode

$$F_1^U = \kappa F(X,t)^2 D_0^2,$$
$$F_1^\theta = C_r \kappa F(X,t)^2 D_0^2. \tag{17}$$

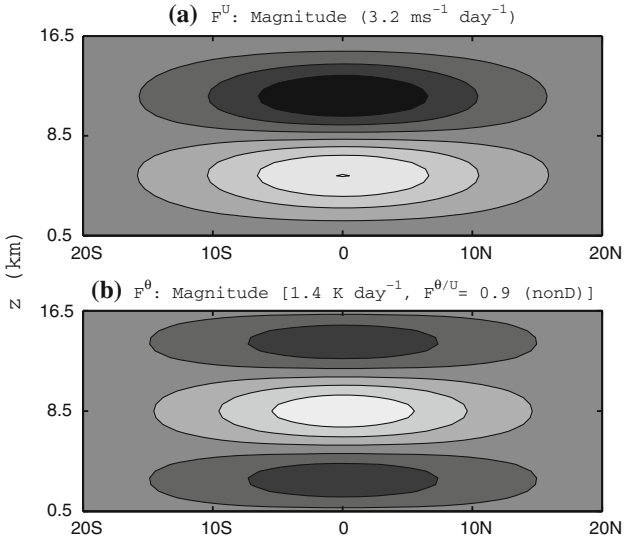

Fig. 2 Eddy momentum transfer (EMT), F^U, and eddy heat transfer (EHT), F^θ, of moist Kelvin waves as functions of y and z. **a** F^U; *white* denotes westerly wind and *black* easterly wind. **b** F^θ; *white* represents positive and *black* negative. The nondimensional magnitude ratio between the EHT and EMT is 0.9. Contour interval is one third of the magnitude and zero contours are not drawn

Keep in mind that F_1^U and F_1^θ have the vertical structures of cos(z) and sin(z), respectively. From Eq. 17, the EHT and EMT have the same horizontal structures. The EMT tends to accelerate the lower-tropospheric westerly winds (Fig. 3a) and the EHT tends to warm up the middle troposphere (Fig. 3b). For the same wave train that has a maximum first baroclinic heating rate of 10 K day^{-1} and a maximum second baroclinic heating rate of 6.7 K day^{-1}, the EMT tends to accelerate the lower troposphere with a magnitude of 2.1 m s^{-1} day^{-1}. The EHT also provides a heating

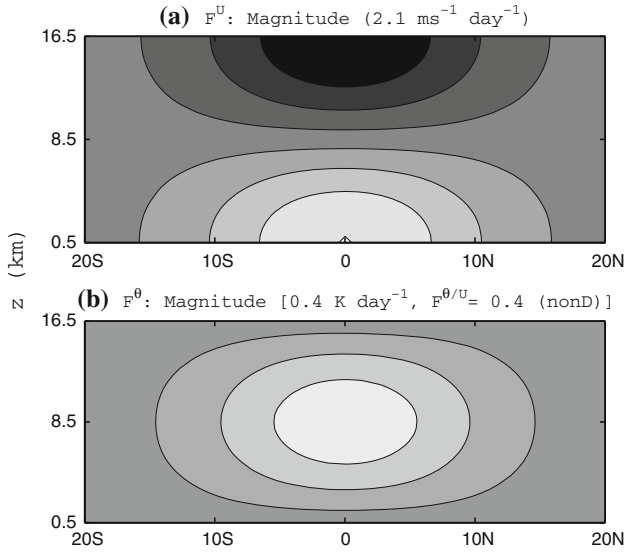

Fig. 3 Same as in Fig. 2 except for the first baroclinic mode. The nondimensional magnitude ratio between the EHT and EMT is 0.4

source for the middle troposphere with a magnitude of 0.4 K day^{-1}. Meanwhile, Eq. 17 shows that the magnitude ratio between the EHT and EMT is determined by the phase speed of moist Kelvin waves, which means that faster moist Kelvin waves produce stronger EHT than the slow movers when compared to the EMT. The strong EHT can provide a considerable instability source for the MJO.

4 Modification of the planetary-scale circulation by the EMT and EHT associated with moist Kelvin waves

By calculating Eq. 4 under different specified forcing centered at 180°, we first explore how the moist Kelvin waves rectify the structure of planetary-scale circulations (Figs. 4, 5). Equation 15 is used for estimating the EMT and EHT. The planetary-scale mean heating rate is defined by

$$S^{\Theta} = \frac{1.5}{0.4} F_1^{\theta}, \tag{18}$$

which means that only the first baroclinic mean heating with magnitude of 1.5 K day^{-1} is included. Equation 4 is calculated by the spectral expansion technique (Majda 2003). The zonal boundary condition is periodic and at the meridional lateral boundaries the fluxes of mass, momentum and heat vanish.

The EMT mainly accelerates the lower-tropospheric westerly winds with their maximum at height 4.5 km (Fig. 4a), consistent with the result forced by superclusters (Majda and Biello 2004; Biello and Majda 2005). A cyclonic pair sandwiches the westerly winds at the lower troposphere (Fig. 5a). These vertical and horizontal structures forced by the EMT is consistent with observations that the westerly wind burst usually occurs at height around 4 or 5 km in the Rossby-gyre region of the active MJO (Lin and Johnson 1996; Moncrieff and Klinker 1997; Houze et al. 2000). However, the winds blowing from the low to high pressure (Figs. 4a, 5a) are not consistent with the wind-pressure relationship in observations (Madden and Julian 1994; Zhang 2005).

Both the EHT and planetary-scale heating tend to warm up the middle troposphere and generate a Gill-like (Gill 1980) pattern (Fig. 5b). In the front of the forcing, the lower-tropospheric easterly winds of the Gill-like response counteract the strong lower-tropospheric westerly winds forced by the EMT (Fig. 4a), and trap the westerly wind burst slightly to the west of the forcing center (Fig. 4d); Meanwhile, the strong equatorial low pressure of the

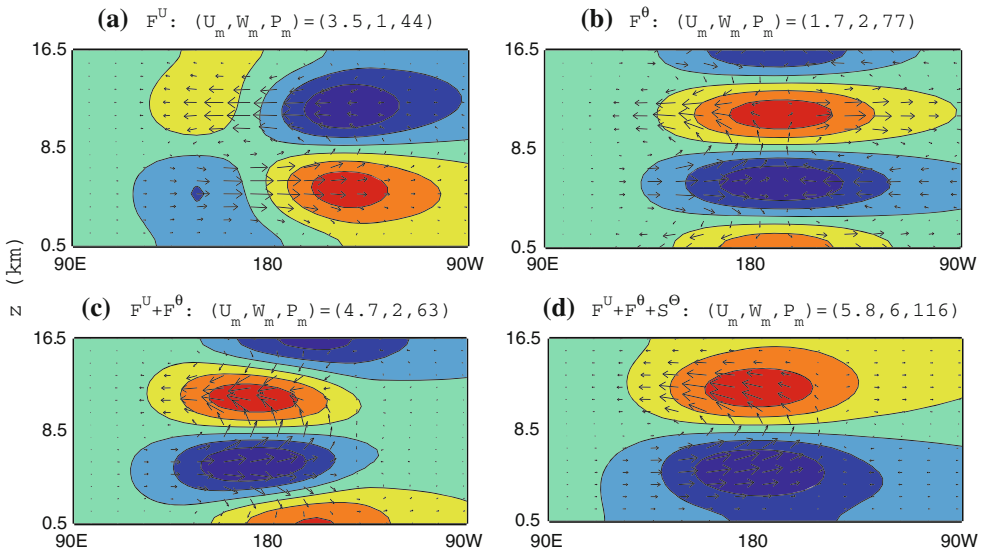

Fig. 4 Vertical structure changes of the equatorial planetary-scale circulations forced by **a** eddy momentum transfer (EMT), F^U, **b** eddy heat transfer (EHT), F^{θ}, **c** both the EMT and EHT, $F^U + F^{\theta}$, and **d** all the EMT, EHT, and planetary-scale mean heating, $F^U + F^{\theta} + S^{\Theta}$. The *red/blue shading* denotes positive/negative pressure and vector the wind. The contour interval is one third of the magnitude and zero contours are not drawn. The units of zonal wind, U_m, vertical velocity, W_m, and pressure, P_m, are m s^{-1}, cm s^{-1}, and m^2 s^{-2}, respectively, where the suffix m denotes the magnitude

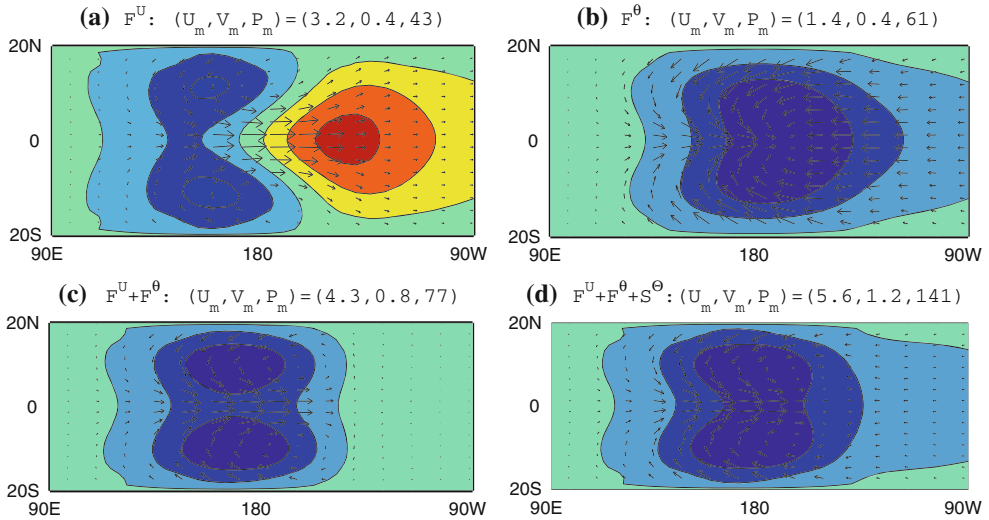

Fig. 5 Horizontal structure rectification of planetary-scale circulations at height 4.5 km forced by **a** eddy momentum transfer (EMT), F^U, **b** eddy heat transfer (EHT), F^θ, **c** both the EMT and EHT, $F^U + F^\theta$, and **d** all the EMT, EHT, and planetary-scale mean heating, $F^U + F^\theta + S^\Theta$. The *red/blue shading* denotes positive/negative pressure and vector the wind. The contour interval is one third of the magnitude and zero contours are not drawn. The units of zonal wind, U_m, meridional wind, V_m, and pressure, P_m, are m s^{-1}, m s^{-1}, and m^2 s^{-2}, respectively, where the suffix m denotes the magnitude

Gill-like response overwhelms the high pressure of the EMT mode (Fig. 5a) in the lower troposphere, and produces equatorial low pressure in the front of the forcing (Fig. 5d). If we assume the MJO convective complex, i.e., the convection center, as an envelope of moist Kelvin waves, these results are consistent with the observation that the lower-tropospheric westerly winds are centered near the center of the MJO heating in the west Pacific and the equatorial lower-tropospheric low pressure exists in the front part of the MJO (Rui and Wang 1990; Madden and Julian 1994; Zhang 2005).

When the planetary-scale mean heating is excluded (Figs. 4c, 5c), the aforementioned two features are weak, but still exist.

5 The MJO-Moist Kelvin wave interaction model

Based on the above results, we further study the role of moist Kelvin waves on the MJO in a scale-interaction model, in which the eddy flux envelope of moist Kelvin waves is no longer pre-specified, but modulated by the MJO.

5.1 The MJO model

The planetary scale (MJO) motion is governed by Eq. 4, in which S^Θ represents the planetary-scale, low-frequency heating rate. Using scale analysis, Wang (1988) has shown that the low-frequency precipitation amount associated with the MJO is only about 20–30% of total precipitation variability, but this amount of planetary-scale heating is sufficient to generate the observed MJO circulation anomalies. To describe moist MJO dynamics, a moisture equation

$$\overline{q}_t - \tilde{Q}\overline{W} = S^q, \tag{19}$$

is added to the planetary-scale Eq. 4, where S^q is the moisture source coming from precipitation, and equals to $-S^\Theta$ for the nondimensional equation. $\tilde{Q}$ is the background vertical moisture gradient and is selected as 0.9 (nondimensional), the standard value for the low-frequency motions (Yano and Emanuel 1991; Frierson et al. 2004).

Following Majda and Stechmann (2009b), the model is formulated in terms of anomalies from a uniform basic state of radiative-convective equilibrium, $\overline{R} = \overline{H}A$, where $\overline{R} = 1\,\mathrm{K\,day^{-1}}$ is the fixed, constant radiative cooling rate, $\overline{H}$ is a constant heating rate. A is a constant (nondimensional) amplitude of wave activity in the equilibrium state. Following Majda and Stechmann (2009b), we assume that the planetary-scale heating anomaly $S^\Theta = \overline{H}\overline{a}$ and $\overline{a}$ is parameterized as:

$$\overline{a}_t = \Gamma\overline{q}(\overline{a} + A), \tag{20}$$

where $\Gamma = 1$ ($\approx 0.2\,\mathrm{K^{-1}\,day^{-1}}$ in dimension) is a constant of proportionality, representing that a positive lower-tropospheric moisture anomaly enhances the planetary-scale heating. The parameterization Eq. 20 is based on a series of observations, in which the lower troposphere tends to be moistened during the suppressed convection phase of the MJO, and the lower-tropospheric moisture leads the MJO's heating anomaly (Myers and Waliser 2003; Kikuchi and

Takayabu 2004; Kiladis et al. 2005; Tian et al. 2006). Keep in mind that in the original skeleton model of Majda and Stechmann (2009b), the wave activity $\overline{a}$ includes both the planetary-scale heating and eddy forcing. Here $\overline{a}$ only represents the planetary-scale heating.

So Eqs. 4, 19 and 20 compose a closed MJO model with the eddy forcing. Because the diabatic heating of the MJO can usually reach higher troposphere, where the Newtonian cooling is important, here we neglect the momentum damping, while keep the Newtonian cooling, as Wang (1988) and Wang and Rui (1990) did. When ignoring the nonlinear term $\Gamma\overline{qa}$ in Eq. 20, we truncate to the first baroclinic mode and obtain the simple scale-interaction model as

$$\begin{aligned}
&\overline{U}_t - y\overline{V} - \overline{\theta}_X = F_1^U,\\
&y\overline{U} - \overline{\theta}_y = 0,\\
&\overline{\theta}_t - \overline{U}_X - \overline{V}_y = \overline{H}\overline{a} + F_1^\theta - d_\theta,\\
&\overline{q}_t + \tilde{Q}(\overline{U}_X + \overline{V}_y) = -\overline{H}\overline{a},\\
&\overline{a}_t = \Gamma A\overline{q}.
\end{aligned} \tag{21}$$

Without the eddy forcing, the EMT, F_1^U and EHT, F_1^θ, and the Newtonian cooling, d_θ, the reduced scale-interaction model Eq. 21 is the same as the original neutral skeleton model (Eq. 3 of Majda and Stechmann 2009b).

5.2 Parameterization of the EMT and EHT

To complete this scale-interaction model Eq. 21, it is necessary to parameterize the EMT and EHT. Since the moist Kelvin waves act as one component of the MJO convective complex, it is natural to assume that the eddy flux envelope, the EMT and EHT, is proportional to the MJO convective complex (planetary-scale heating): both the zonal and meridional structures of the eddy flux envelope have the same form as the planetary-scale heating, and their amplitude is also proportional to the heating strength. As a scale-interaction model, the eddy fluxes would be nonlinear, while in order to obtain a simple linear scale-interaction model, we only use this linear relationship. So Eq. 17 is parameterized as

$$\begin{aligned}
&F_1^\theta = C_\theta \overline{H}\overline{a},\\
&F_1^U = C_r^{-1} F_1^\theta.
\end{aligned} \tag{22}$$

C_θ is an arbitrary coefficient associated with the EHT, while we can parameterize it based on the relationship obtained in the above results: On the first baroclinic mode, the standard moist Kelvin waves with heating rate of 10 K day^{-1} at its maximum can produce an EHT with magnitude of 0.4 K day^{-1}, i.e., $F_1^\theta = C_\theta\overline{H}\overline{a} \approx 0.4$ K day^{-1}; the heating rate with magnitude of 1.5 K day^{-1}, $\overline{H}\overline{a} \approx 1.5$ K day^{-1}, is reasonable for the observed MJO (Lin and Johnson 1996; Yanai et al. 2000). Divide these two relationships we can obtain an assumption of $C_\theta \approx 0.4/1.5 = 0.27$.

5.3 Eigenvalue problem

Equations 21 and 22 compose a set of linear partial differential equations, which can be solved as an Eigenvalue problem. For the plane waves, we assume that they have the structure of $e^{i(\mathrm{K}X-\sigma t)}$, where K is the wavenumber and σ is the frequency. The phase speed and growth rate are defined by Re(σ)/K and Im(σ), respectively. When only the lowest N modes of each variable are kept for the meridional expansion of parabolic cylinder functions, we project Eqs. 21–22 on the σ − K space, and obtain a linear matrix of (5N × 5N) for the five variables in Eq. 21. Here N = 1 represents the lowest equatorially trapped mode. The frequency σ and eigenvectors are calculated through the matrix inversion corresponding to each wavenumber K. Only the Kelvin and Rossby waves are remained in Eq. 21 because of the long wave approximation. Following the idea that the planetary-scale heating only has the lowest meridional truncation of parabolic cylinder functions (Majda and Stechmann 2009b), the Rossby and Kelvin waves on their lowest meridional modes can be studied by using N = 3, and sensitive experiments show that higher N does not affect the results.

6 Instability and eastward propagation mechanisms for the modeled MJO

Without the eddy forcing and Newtonian cooling, this model is reduced to the neutral skeleton model of Majda and Stechmann (2009b), and the results recover their solutions, which consist of two families of low-frequency (above 30 days) eigenmodes, one propagates slowly eastward and the other westward (Fig. 6b, c). These two groups of modes all have zero growth rates (Fig. 6a), hence, there is no preferred eastward propagation. In the presence of eddy forcing from moist Kelvin waves, however, both EHT and EMT can destabilize MJO motions and only eastward propagating modes become unstable (Fig. 6a), which become the preferred dominant modes. The coupled EHT and EMT present a stronger instability for the eastward MJO than they act alone (Fig. 6a), and they also select the long eastward propagating modes to grow up against the tropospheric damping. This explains why the low-frequency MJO has prevailing eastward propagation.

Why does the eddy forcing only destabilize eastward propagating modes? Since the EHT of moist Kelvin waves

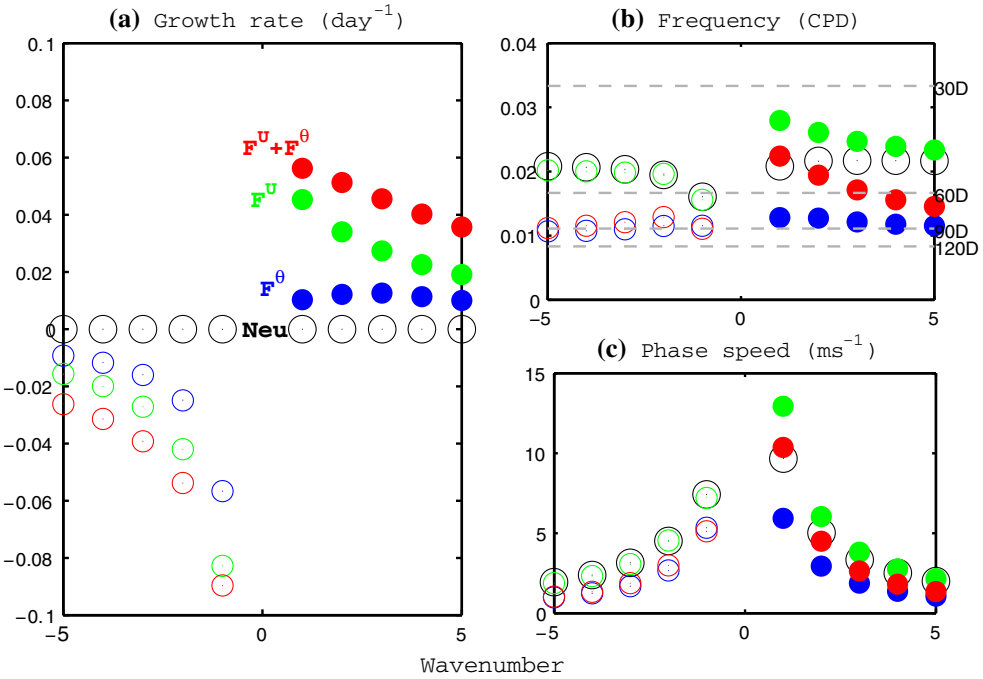

Fig. 6 Solutions of the linear scale-interaction model. Growth rate (**a**), frequency (**b**), and phase speed (**c**) as functions of wavenumber. Growing modes are denoted by *solid dots* and damped or neutral modes are denoted by *empty circles*. The results coming from the neutral (Neu), EHT (F^{θ}), EMT (F^{U}), and coupled EHT and EMT ($F^{U} + F^{\theta}$) modes are colored by *dark*, *blue*, *green*, and *red*, respectively

tends to warm up the middle troposphere and increases the positive temperature anomaly, it does provide an instability source for the MJO mode. Under the current parameters, wavenumber 3 has the strongest instability (Fig. 6a). The EMT also provides an instability source for the eastward MJO, especially for the long waves (Fig. 6a), because it favors acceleration of the lower-tropospheric westerly winds of the MJO. The generation of the perturbation available potential energy (APE) requires a positive covariance between the perturbation temperature and diabatic heating (Wang and Rui 1990). For neutral mode, the perturbation heating and temperature have a $\pi/2$ phase difference (Fig. 7a), so no APE can be generated. The westerly EMT and EHT-induced heating, either separately or together, change the horizontal temperature and heating structures of the westward (Fig. 7b) and eastward (Fig. 7c)

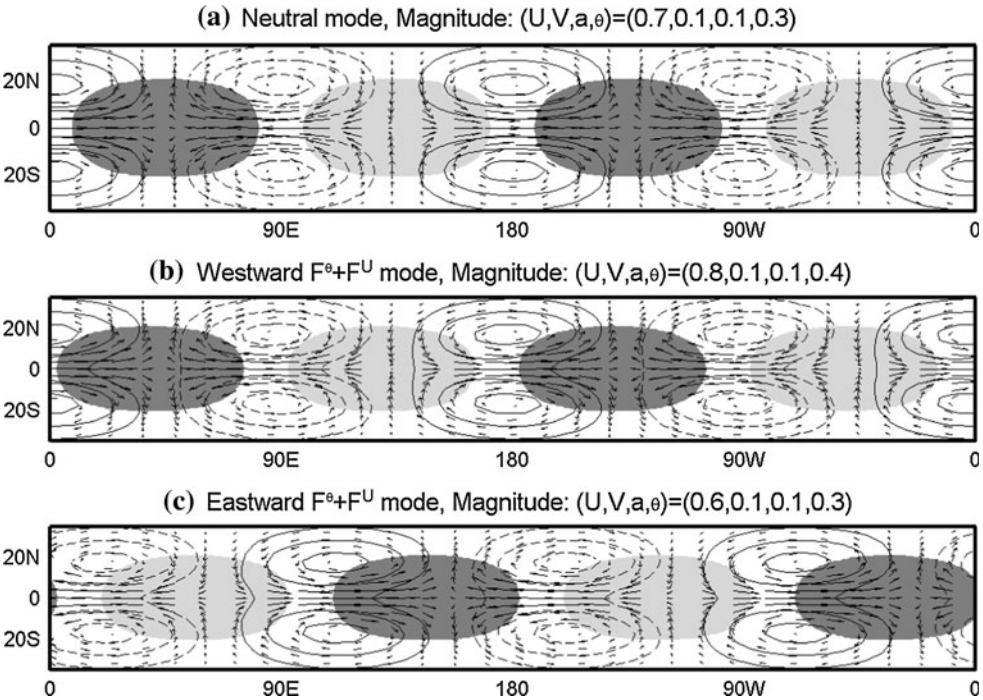

Fig. 7 Dynamic structures of different modes with wavenumber two. Velocity (*vectors*) and temperature (*contours*), as well as planetary-scale heating (*shading*) are drawn for the neutral (**a**), westward (**b**) and eastward (**c**) scale-interaction modes, respectively. Positive (negative) contours are solid (*dashed*), and positive (negative) shading is dark (*gray*). Contour interval is one third of the magnitude and zero contours are not drawn. Only heating rate above one third of the magnitude is *shaded*

modes. For eastward mode, the perturbation heating leads the positive temperature anomaly by a phase between $\pi/4$ and $\pi/2$ (Fig. 7c), thus positive APE has been generated. In contrast, for westward mode, the perturbation heating leads the positive temperature anomaly by a phase that is a little smaller than $\pi/2$, while their negative covariance dominates near the equator, generating negative APE (Fig. 7b). Therefore, only the eastward propagating mode is a growing and preferred mode.

In addition to the growth rate, the eddy forcing also modifies the phase speed of eastward MJO modes. The inclusion of the EHT will slow down the eastward MJO modes (Fig. 6b, c), because the heating source of the EHT in the middle troposphere will increase the convective APE and reduces the equivalent depth (Gill 1980; Kiladis et al. 2009). The EMT tends to speed up the eastward MJO modes (Fig. 6b, c), especially the long waves. The reason is the advective shift of lower-tropospheric westerly wind acceleration of the EMT.

7 Summary and discussion

7.1 Importance of the eddy transfer of moist Kelvin waves to MJO dynamics

The new results obtained from the present model indicate that the moist Kelvin waves exhibit considerable eddy heat transfer (EHT), which warms up the middle troposphere and induces weak lower-tropospheric easterly winds and low pressure in the front of the MJO. This seems to be more consistent with the observed features of the MJO (Rui and Wang 1990; Madden and Julian 1994; Zhang 2005).

Both the moist Kelvin wave-induced EHT and eddy momentum transfer (EMT) can destabilize the planetary-scale MJO motion. The EHT provides an instability source for the MJO by warming the middle troposphere, and tends to slow down the MJO. The EMT provides an additional instability source for the MJO by accelerating the lower-tropospheric westerly winds of the MJO and tends to speed up the MJO by its advective shift.

Of particular interest is that the eddy forcing can select the eastward propagation for the unstable MJO modes, because the eddy forcing generates positive/negative available potential energy (APE) for the eastward/westward modes by changing their thermal and dynamical structures.

7.2 Implications

Based on these results, we can further study the role of the phase relation between moist Kelvin waves and the MJO, because the moist Kelvin waves are usually observed to travel through the MJO (Roundy 2008; Kikuchi and Wang 2010). For the plane-wave structure, we assumed, in Sect. 5, that the eddy flux envelope has the same structure as the convective complex (planetary-scale heating) of the MJO.

In order to examine how the effect of moist Kelvin waves depends on their relative locations with respect to the MJO, here we assume that the eddy flux envelope leads the convective complex center by a phase of γ, so Eq. 22 becomes

$$F_1^{\theta} = \mathrm{Re}(C_{\theta}\overline{H\alpha}e^{-i\gamma}),$$
$$F_1^{U} = \mathrm{Re}(C_r^{-1}C_{\theta}\overline{H\alpha}e^{-i\gamma}). \quad (23)$$

By the same method, we recalculate Eqs. 21 and 23. For convenience of comparison, the unstable MJO mode with wavenumber two is displayed. Figure 8 shows that only when appearing near the convective complex center of the MJO, can the moist Kelvin waves provide a positive feedback in sustaining the MJO. The moist Kelvin waves propagating away from the MJO convective center, especially to the west of the MJO, may damp the MJO.

Compared to the standard moist Kelvin waves (with a speed of 18 m s^{-1}) that have a magnitude ratio of eddy flux of $F_1^{\theta}/F_1^{U} = 0.36$ (Fig. 9b), the fast moist Kelvin waves (with a speed of 25 m s^{-1}) have relative strong EHT compared to the EMT, $F_1^{\theta}/F_1^{U} = 0.5$, and the most unstable MJO occurs when the eddy flux envelope appears to the east of the convective center of the MJO (Figs. 8, 9a), the reason is that the instability mainly comes from the EHT, which tends to warm up the middle troposphere and increases the convective APE in the front of the MJO (Lin and Johnson 1996; Wang and Xie 1998). On the other

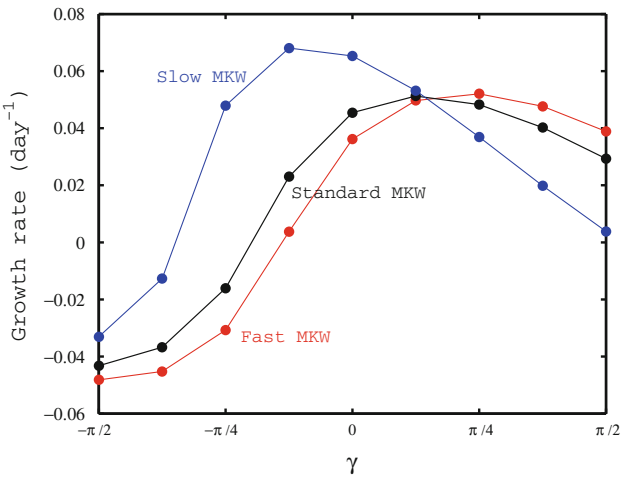

Fig. 8 Growth rate as a function of leading phase γ between the eddy flux envelope and convective complex of the MJO with wavenumber 2, which is forced by the moist Kelvin waves (MKW) with phase speeds of 25, 18 and 10 m s^{-1}, respectively

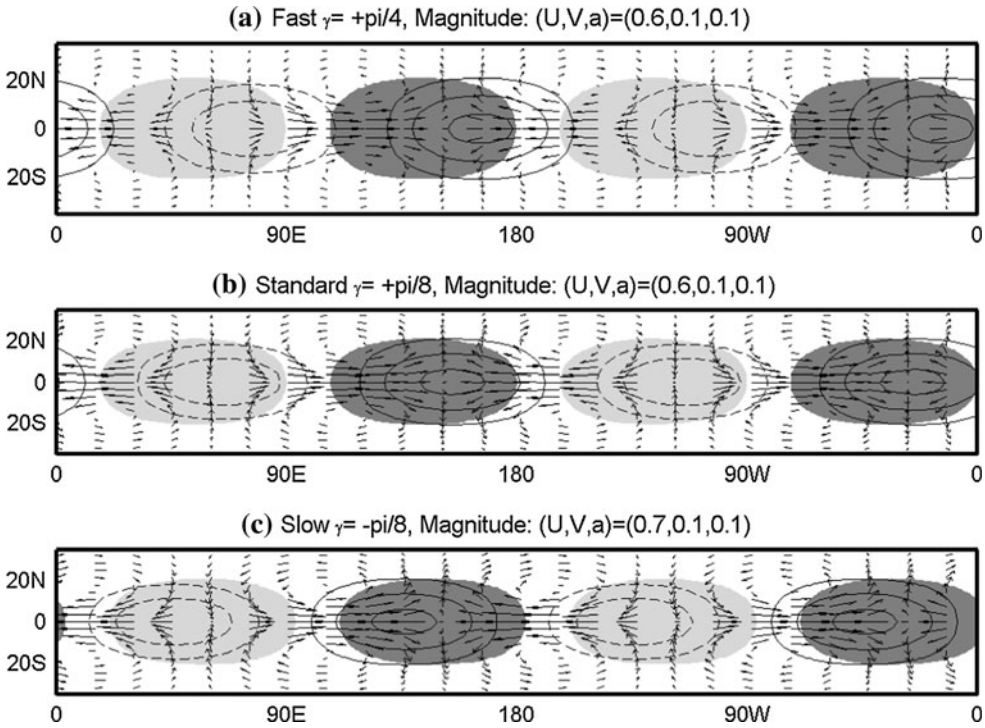

Fig. 9 Dynamic structures of different modes in Fig. 8. Velocity vectors with eddy flux envelope (*contours*) and planetary-scale heating (*shading*) of the MJO that are forced by **a** the fast (25 m s^{-1}) moist Kelvin waves with $\gamma = \pi/4$, **b** the standard (18 m s^{-1}) moist Kelvin waves with $\gamma = \pi/8$, and **c** the slow (10 m s^{-1}) moist Kelvin waves with $\gamma = -\pi/8$. Positive (negative) contours are solid (*dashed*), and positive (negative) shading is dark (*gray*). Contour interval is one third of the magnitude and zero contours are not drawn. Only heating rate above one third of the magnitude is *shaded*

hand, when the moist Kelvin waves are slow (with a speed of 10 m s^{-1}), the EHT is relative small, $F_1^{\theta}/F_1^{U} = 0.2$. Figures 8 and 9c show that the most unstable MJO occurs when the moist Kelvin waves are enhanced to the west of the convective center of the MJO, where the instability mainly comes from the impact of the EMT that accelerates the lower-tropospheric westerly winds of the MJO. This result agrees with the previous works (Wang and Liu 2011; Liu et al. 2011) that the superclusters in the rear part of the MJO can provide an instability source for the MJO.

The dynamical results emphasize the important roles of moist Kelvin waves in different part of the MJO, and encourage more observations on the cloud structures and intensities of moist Kelvin waves associated with different phases of the MJO.

7.3 Limitation of this work

In order to obtain this simple linear scale-interaction model, a linear assumption on the eddy flux envelope was made (Sect. 5.2), and sensitivity experiments show that a strong planetary-scale heating in this assumption will enhance the role of the eddy forcing linearly. This assumption is too simple and cannot account for nonlinear scale interaction. A nonlinear eddy flux effect should be implemented into the MJO model in the future works.

Although this scale-interaction model presented a wave selection of wavenumber one that is most unstable for the MJO, this wave selection is parameter dependent. With very strong EHT and EMT, this model will yield stronger growth rates on shorter wavelengths (Figure not shown). Hence we de-emphasize the role of upscale fluxes from moist Kelvin waves on the long wave selection for the MJO. In the future work, we will show that the inclusion of planetary boundary layer will offer a good explanation for this long wave selection mechanism in terms of growth rate.

The skeleton model produces a model MJO that has no vertical tilt. This is at odds with observed vertical structure of the MJO. New physical processes need to be implemented into the model to account for this essential feature.

Acknowledgments The authors thank two anonymous reviews for their comments and suggestions. This study was supported by Climate Dynamics Program of the National Science Foundation under award No AGS-1005599 and Global Research Laboratory (GRL) Program from the Ministry of Education, Science, and Technology (MEST), Korea. Additional support was provided by the Japan Agency for Marine-Earth Science and Technology (JAMSTEC), by NASA through grant NNX07AG53G, and by NOAA through grant NA17RJ1230 through their sponsorship of research activities at the International Pacific Research Center. This paper is the SOEST Contribution No. 8551 and IPRC publication No. 839.

References

Biello JA, Majda AJ (2005) A new multiscale model for the Madden–Julian oscillation. J Atmos Sci 62:1694–1721

Biello JA, Majda AJ (2006) Modulating synoptic scale convective activity and boundary layer dissipation in the IPESD models of the Madden-Julian oscillation. Dyn Atmos Oceans 42:152–215

Frierson D, Majda AJ, Pauluis O (2004) Dynamics of precipitation fronts in the tropical atmosphere. Comm Math Sci 2:591–626
Gill AE (1980) Some simple solutions for heat-induced tropical circulation. Q J R Meteor Soc 106:447–462
Haertel PT, Kiladis GN (2004) Dynamics of 2-Day equatorial waves. J Atmos Sci 61:2707–2721
Houze RA Jr, Chen SS, Kingsmill DE, Serra Y, Yuter SE (2000) Convection over the Pacific warm pool in relation to the atmospheric Kelvin–Rossby wave. J Atmos Sci 57:3058–3089
Khouider B, Majda AJ (2006) A simple multicloud parameterization for convectively coupled tropical waves. Part I: linear analysis. J Atmos Sci 63:1308–1323
Khouider B, Majda AJ (2007) A simple multicloud parameterization for convectively coupled tropical waves. Part II. Nonlinear simulations. J Atmos Sci 64:381–400
Kikuchi K, Takayabu YN (2004) The development of organized convection associated with the MJO during TOGA COARE IOP: trimodal characteristics. Geophys Res Lett 31:L10101. doi:10.1029/2004GL019601
Kikuchi K, Wang B (2010) Spatiotemporal wavelet transform and the multiscale behavior of the Madden–Julian oscillation. J Clim 23:3814–3834
Kiladis GN, Straub KH, Haertel PT (2005) Zonal and vertical structure of the Madden–Julian oscillation. J Atmos Sci 62:2790–2809
Kiladis GN, Wheeler MC, Haertel PY, Straub KH, Roundy PE (2009) Convectively coupled equatorial waves. Rev Geophys 47:RG2003
Lin X, Johnson RH (1996) Kinematic and thermodynamic characteristics of the flow over the western Pacific warm pool during TOGA COARE. J Atmos Sci 53:695–715
Liu F, Wang B (2011) A model for the interaction between the 2-day waves and moist Kelvin waves. J Atmos Sci. doi:10.1175/JAS-D-11-0116.1
Liu F, Huang G, Feng L (2011) Critical roles of convective momentum transfer in sustaining the multi-scale Madden-Julian oscillation. Theor Appl Climatol. doi:10.1007/s00704-011-0541-6
Madden R, Julian P (1971) Detection of a 40–50 day oscillation in the zonal wind in the tropical Pacific. J Atmos Sci 28:702–708
Madden R, Julian P (1972) Description of global-scale circulation cells in the tropics with a 40–50 day period. J Atmos Sci 29:1109–1123
Madden R, Julian P (1994) Observations of the 40–50-day tropical oscillation—a review. Mon Weather Rev 122:814–837
Majda AJ (2003) Waves and PDEs for the equatorial atmosphere and ocean. Introduction to PDEs and waves for the Atmosphere and Ocean, Courant Institute Lecture Series 9. American Mathematical Society, pp 199–232
Majda AJ, Biello JA (2004) A multiscale model for the intraseasonal oscillation. Proc Natl Acad Sci USA 101:4736–4741
Majda AJ, Klein R (2003) Systematic multiscale models for the tropics. J Atmos Sci 60:393–408
Majda AJ, Stechmann SN (2009a) A simple dynamical model with features of convective momentum transport. J Atmos Sci 66:373–392
Majda AJ, Stechmann SN (2009b) The skeleton of tropical intraseasonal oscillations. Proc Natl Acad Sci USA 106:8417–8422
Mapes BE (2000) Convective inhibition, subgrid-scale triggering energy, and stratiform instability in a toy tropical wave model. J Atmos Sci 57:1515–1535
Matsuno T (1966) Quasi-geostrophic motions in the equatorial area. J Meteorol Soc Jpn 44:25–43
Moncrieff MW (2004) Analytic representation of the large-scale organization of tropical convection. J Atmos Sci 61:1521–1538
Moncrieff MW, Klinker E (1997) Organized convective systems in the tropical western Pacific as a process in general circulation models: a TOGA COARE case study. Q J R Meteor Soc 123:805–827
Myers D, Waliser D (2003) Three-dimensional water vapor and cloud variations associated with the Madden–Julian oscillation during Northern Hemisphere winter. J Clim 16:929–950
Nakazawa T (1988) Tropical super clusters within intraseasonal variations over the western Pacific. J Meteor Soc Jpn 66:823–836
Roundy PE (2008) Analysis of convectively coupled Kelvin waves in the Indian Ocean MJO. J Atmos Sci 65:1342–1359
Rui H, Wang B (1990) Development characteristics and dynamic structure of tropical intraseasonal convection anomalies. J Atmos Sci 47:357–379
Straub KH, Kiladis GN (2003) Interactions between the boreal summer intraseasonal oscillation and higher-frequency tropical wave activity. Mon Weather Rev 131:945–960
Takayabu YN, Murakami M (1991) The structure of super cloud clusters observed in 1–20 June 1986 and their relationship to easterly waves. J Meteor Soc Jpn 69:105–125
Tian B, Waliser D, Fetzer E, Lambrigtsen B, Yung Y, Wang B (2006) Vertical moist thermodynamic structure and spatial–temporal evolution of the MJO in AIRS observations. J Atmos Sci 63:2462–2485
Waite ML, Khouider B (2009) Boundary layer dynamics in a simple model for convectively coupled gravity waves. J Atmos Sci 66:2780–2795
Wang B (1988) Dynamics of tropical low-frequency waves: an analysis of the moist Kelvin wave. J Atmos Sci 45:2051–2065
Wang B, Liu F (2011) A model for scale interaction in the Madden-Julian oscillation. J Atmos Sci. doi:10.1175/2011JAS3660.1
Wang B, Rui H (1990) Dynamics of coupled moist Kelvin-Rossby waves on an equatorial beta-plane. J Atmos Sci 47:397–413
Wang B, Xie X (1998) Coupled modes of the warm pool climate system. Part I: the role of air-sea interaction in maintaining Madden–Julian oscillation. J Clim 11:2116–2135
Wheeler M, Kiladis GN (1999) Convectively coupled equatorial waves: analysis of clouds and temperature in the wavenumber-frequency domain. J Atmos Sci 56:374–399
Yanai M, Chen B, Tung WW (2000) The Madden–Julian oscillation observed during the TOGA COARE IOP: global view. J Atmos Sci 57:2374–2396
Yano JI, Emanuel KA (1991) An improved model of the equatorial troposphere and its coupling to the stratosphere. J Atmos Sci 48:377–389
Zhang C (2005) Madden-Julian oscillation. Rev Geophys 43:RG2003. doi:10.1029/2004RG000158